Hindawi
Geofluids
Volume 2022, Article ID 8978653, 19 pages
https://doi.org/10.1155/2022/8978653

Research Article

Establishment and Application of Bed-Separation Water Inrush Coefficient Method Considering Water Resistance of Fractured Rock Mass

Jianghui He,[1,2] **Wenping Li**,[3] **Wei Qiao**,[3] **Qiqing Wang**,[3] **Zhi Yang**,[4] **and Liangning Li**[3]

[1]*State Key Laboratory of Mining Response and Disaster Prevention and Control in Deep Coal Mines, Anhui University of Science and Technology, Huainan 232001, China*
[2]*School of Earth and Environment, Anhui University of Science and Technology, Huainan 232001, China*
[3]*School of Resources and Geosciences, China University of Mining & Technology, Xuzhou 221116, China*
[4]*School of Environment and Spatial Informatics, China University of Mining & Technology, Xuzhou 221116, China*

Correspondence should be addressed to Wenping Li; hjh@cumt.edu.cn

Received 6 September 2021; Accepted 24 February 2022; Published 25 March 2022

Academic Editor: Yong-Zheng Wu

Deep mining in Ordos Basin faces the threat of bed-separation water inrush (BWI), so it is necessary to carry out BWI risk assessment before mining. However, the existing BWI risk assessment methods fail to provide a universal risk classification standard. In this paper, taking three coal mines in Ordos Basin as research cases, the water resistance of fractured rock mass was analyzed, and a BWI coefficient (*BWIC*) method for BWI risk assessment was established. Firstly, by comparing the weight of each BWI-related factor, the formula for calculating the thickness of equivalent water-resisting layer of fractured rock mass was derived. The weight of each BWI-related factor was obtained by entropy weight method. Secondly, based on the stress arch theory, the overall *BWIC* in bed separation zone corresponding to different excavation lengths was obtained. *BWIC* was expressed by the ratio of the Cretaceous water pressure to the total thickness of the unbroken water-resisting layer and the equivalent water-resisting layer of the fractured rock mass. Finally, by comparing the value range of the overall *BWIC* in the bed separation zone corresponding to the excavation length with and without BWI, the standard of BWI risk classification was determined. The application results verified the scientificity of *BWIC* method and the universality of the BWI risk classification standard proposed in this paper.

1. Introduction

Bed separation is a layered cavity formed between adjacent strata due to uneven settlement of strata in overburden during underground coal mining [1–5]. When the water in the surrounding aquifer accumulates into the bed separation, bed-separation water is formed. Once the bed-separation water breaks through the water-resisting layer below it and flows into the mining site, it will cause bed-separation water inrush (BWI) [6]. BWI has the characteristics of large instantaneous water volume and strong destructiveness. Coal is still the most important fossil energy in China, and Ordos Basin has become China's main coal producing area [7, 8]. In underground coal mining, because China has the most complex geological conditions and the largest coal mining scale in the world, almost all accidents caused by BWI occur in China. For example, in 2016, a BWI occurred at Zhaojin coal mine in China, resulting in 11 deaths. Therefore, for those coal mines facing BWI threat in Ordos Basin, BWI risk assessment has important reference value for the formulation of safe mining scheme.

At present, mine engineers still have different views on the formation mechanism of BWI. Some views are that the power to induce BWI comes from the impact of the fracture of the rock stratum constituting the bed separation on the bed-separation water [9–11], while some views are that the bed-separation water pressure is the power to drive the bed-separation water to break through the aquiclude [12, 13]. In

fact, in the overburden, the inrush of bed-separation water in the fracture zone should be caused by the fracture of rock stratum, but the inrush of bed-separation water above the fracture zone should be driven by bed-separation water pressure. Although BWI is not a new type of roof water hazards in coal mining in recent years, but due to the lack of attention, there are few research results on risk assessment of BWI. Multifactor-weighted superposition method is a mature risk assessment method, and it is often used in mine roof/floor water inrush risk assessment [14, 15]. However, in the multifactor-weighted superposition method, the result of data standardization processing will be affected by the value range of the data set, which will lead to the BWI risk may be wrongly evaluated and the boundary values between different risk levels changing with the change of evaluation area, for example, assuming that the values of one of the BWI-related factors in mining areas A and B are data set $A = \{a_1, a_2, \cdots, a_i, \cdots, a_m\}$ and data set $B = \{b_1, b_2, \cdots, b_j, \cdots, b_n\}$, respectively. The maximum and minimum values in data set A are $a_{\max}$ and $a_{\min}$, respectively, and the maximum and minimum values in data set B are $b_{\max}$ and $b_{\min}$, respectively. The value of the BWI-related factor at coordinate point X in mining area A is a_x, and the value of the BWI-related factor at coordinate point Y in mining area B is b_y, and $a_x = b_y$. If $a_{\max} = b_{\max}$ and $a_{\min} = b_{\min}$ cannot exist at the same time, the standardized values of a_x and b_y will not be equal, and the BWI risk at coordinate point X and coordinate point Y will be evaluated as unequal, which is not in line with the reality. The water inrush coefficient method, which was improved from the empirical formula suitable for floor water inrush risk assessment and suitable for roof water inrush risk assessment, has been used in BWI risk assessment [16]. However, the evaluation results were not convincing because the water-resisting capacity of the fractured Jurassic strata in Ordos Basin due to the fracture self-healing effect was not considered.

The above analysis shows that there is still a lack of practical methods suitable for BWI risk assessment in Ordos Basin. Moreover, the BWI risk corresponding to different excavation lengths cannot be obtained by using the existing BWI risk assessment methods, which is not conducive to guiding relevant disaster prevention and control. Therefore, the purpose of this paper is to analyze the role of BWI-related factors in BWI and establish a BWI risk assessment method that can provide water inrush risk corresponding to different excavation lengths and universal risk classification standard.

2. Engineering Geological Background of Coal Mining in Ordos Basin

Ordos Basin is the main coal producing area in China, and Jurassic coal seams are the main excavation objects. In the middle of the basin, a thick layer of Cretaceous strata is deposited above the Jurassic Anding Formation (Figure 1). The Cretaceous strata are mainly composed of thick sandstone with a small amount of sandy mudstone intercalation, which has good integrity (Figures 2 and 3(a)) and is not easy to deform, while the Jurassic Anding Formation is mainly composed of mudstone and sandy mudstone and has weathering zone inside, which is easy to deform (Figures 3(b) and 4). In the subsidence caused by underground mining, due to the asynchronous deformation between sandstone and sandy mudstone in Cretaceous and between Cretaceous and Jurassic Anding Formation, layered cavities (i.e., bed separations) appear in Cretaceous and the interface between Cretaceous and Jurassic Anding Formation (Figure 5). When the water in the aquifer around a bed separation converges into the bed separation, bed-separation water is formed, which can lead to the decline of the water level in the surrounding aquifer (Figure 6). When the bed-separation water suddenly burst into the mining area, BWI is formed. Due to the deformation of sandy mudstone intercalation in Cretaceous is clamped by its adjacent thick sandstone layers, bed separations in Cretaceous have smaller scale. On the contrary, because the overall antideformation ability of Cretaceous is greater than that of Jurassic Anding Formation, the deformation difference between Cretaceous and Jurassic Anding Formation is larger; bed separations at the interface of Cretaceous and Jurassic Anding Formation have larger scale. Therefore, the bed-separation water at the interface between Cretaceous and Jurassic Anding Formation is the focus of this study.

3. Methods and Materials

3.1. BWI-Related Factors and Their Quantification. As shown in Figure 5, BWI is caused by the breakthrough of the Jurassic protective layer by the Cretaceous bed-separation water above it. Therefore, the research objects directly involved in BWI process include the Cretaceous bed-separation water and the Jurassic protective layer. In the Jurassic protective layer, the upper part is the unbroken Jurassic strata (UJS), and the lower part is the fractured Jurassic strata (FJS). The water-resisting capacity of FJS is due to the closure of fractures in FJS under the action of water flow. Furthermore, the strata in FJS can be divided into fractured mudstone and fractured sandstone. The role and quantification of each BWI-related factor in BWI are described below.

(1) Bed-separation water pressure (P_b)

The bed-separation water pressure (P_b) provides the inducing power for the occurrence of BWI. Since the bed-separation water comes from the aquifer around the bed separation, when the bed separation is filled with water, P_b will gradually increase to be consistent with the water pressure in the aquifer around the bed separation. Since the bed separations at the interface between Cretaceous and Jurassic strata are the focus of this study, in this study, the Cretaceous P_b can be expressed by the water pressure in the aquifer at the bottom of Cretaceous.

(2) UJS thickness (T_U)

UJS is the key factor affecting BWI because it can prevent the release of bed-separation water. Because the integrity of UJS is not damaged, it has greater strength and

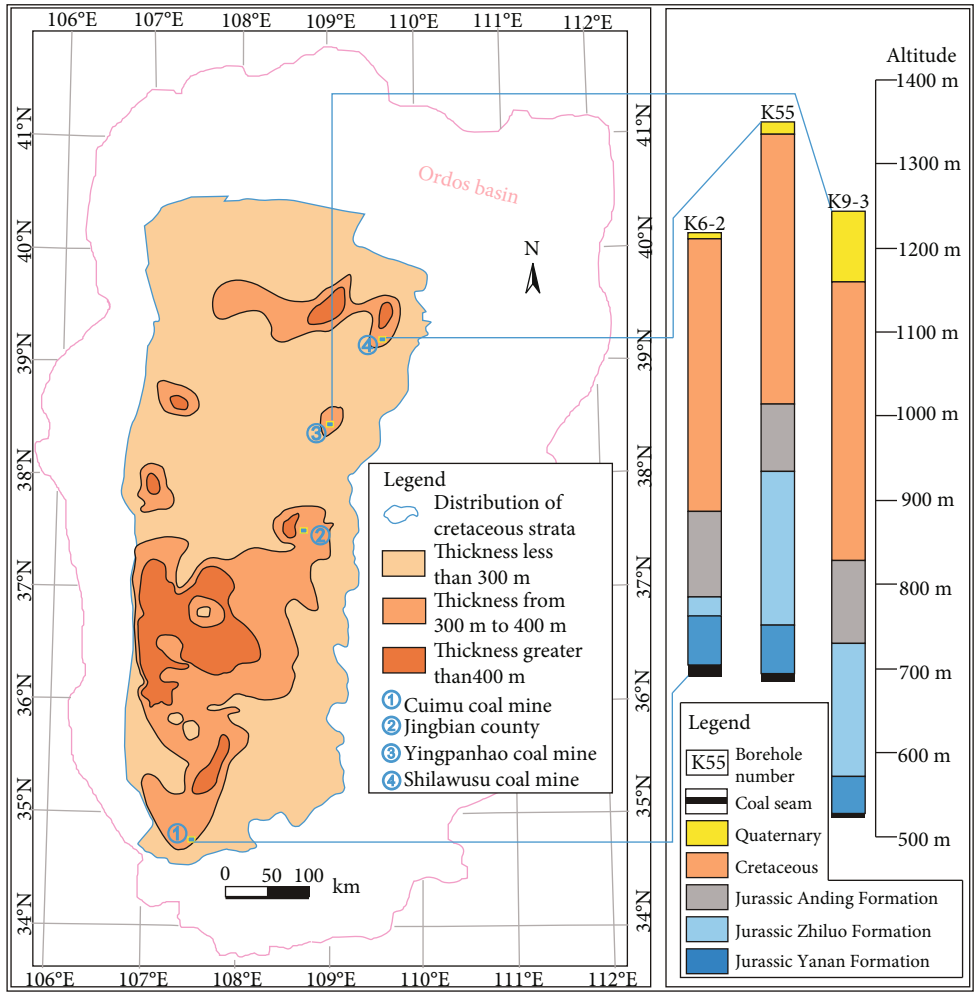

Figure 1: Engineering geological background in the study area.

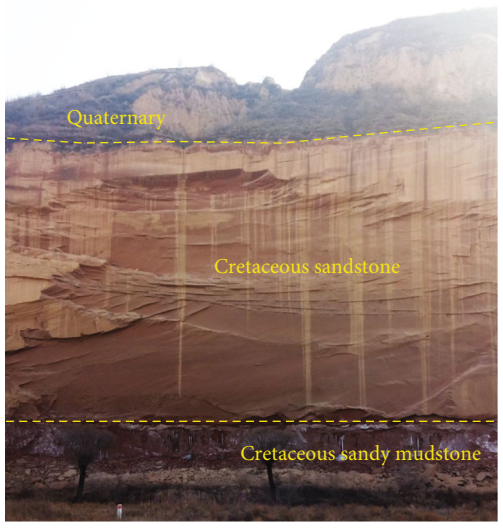

Figure 2: Outcrop of Cretaceous strata (December 2018, Jingbian, China).

better water-resisting capacity than FJS. The greater the thickness of UJS (T_U) is, the stronger its water-resisting capacity is. T_U can be calculated as follows:

$$T_U = T_J - T_F, \tag{1}$$

$$T_F = M * R_{FM}, \tag{2}$$

where T_J is the thickness of Jurassic strata between coal seam and Cretaceous (that is, the thickness of Jurassic protective layer); T_F is the thickness of FJS; M is the mining thickness; and R_{FM} is the ratio of T_F and M, which can be obtained through field monitoring.

(3) Closure potential of mudstone fractures in FJS (C_m)

Due to the low strength (with an average saturated uniaxial compressive strength of 4.75 MPa) and low softening coefficient (with an average softening coefficient of 0.34), the Jurassic mudstone can be easily argillated and deformed after encountering water (Figure 7), resulting in the self-healing effect of fractures in Jurassic mudstone under the action of water flow.

(a) (b)

Figure 3: Rock cores drilled in the Yingpanhao mine of (a) Cretaceous strata and (b) the Jurassic Anding Formation.

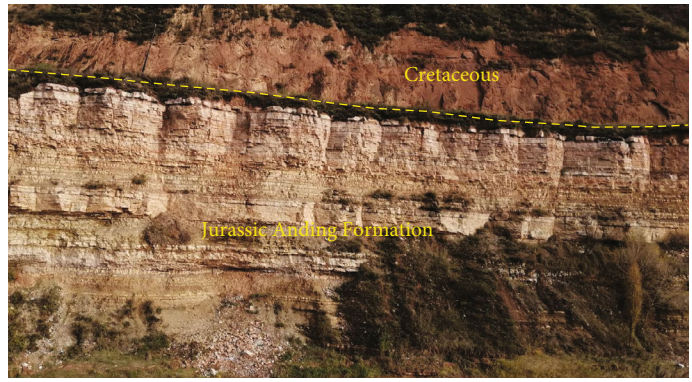

Figure 4: Outcrop of the interface between Cretaceous strata and the Jurassic Anding Formation in the Ordos Basin (October 2019, Jingbian, China).

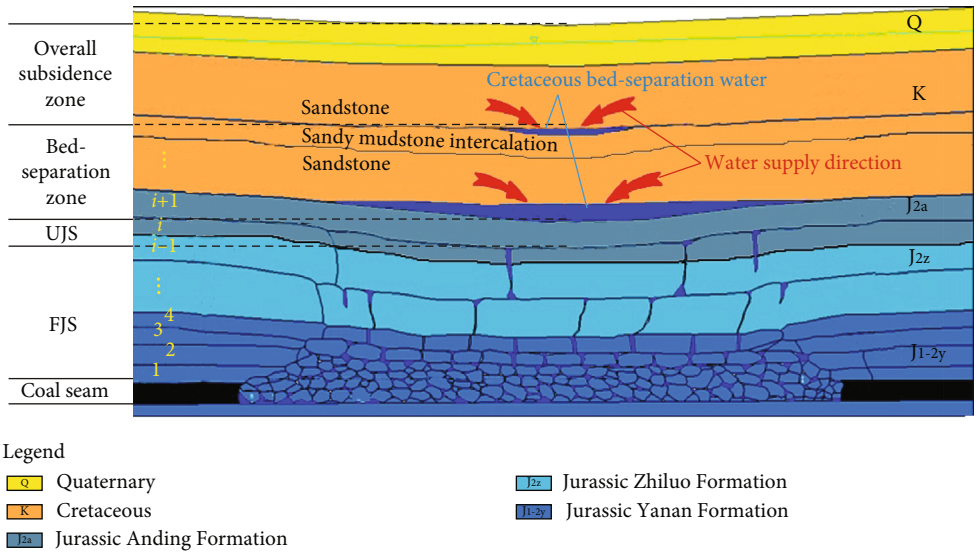

Figure 5: Schematic diagram of Cretaceous bed-separation water formation and mining disturbed overburden zoning during Jurassic coal seam mining: T_i: total thickness of all strata between the i^{th} layer and the coal seam.

In FJS, the better the closure effect of mudstone fractures, the stronger the water-resisting capacity of mudstone, and the smaller the probability of BWI. Here, the closure potential of mudstone fractures in FJS (C_m) was used to evaluate the closure effect of mudstone fractures. Because C_m is positively correlated with the volume of mudstone and the volume of mudstone is positively correlated with the mudstone thickness, C_m is positively correlated with the mudstone thickness. On the contrary, because C_m is negatively correlated with the opening degree of mudstone fractures, and the opening degree of mudstone fractures is positively correlated with the height of available subsidence space of mudstone before mudstone fracture, C_m is negatively correlated with the height of available subsidence space of

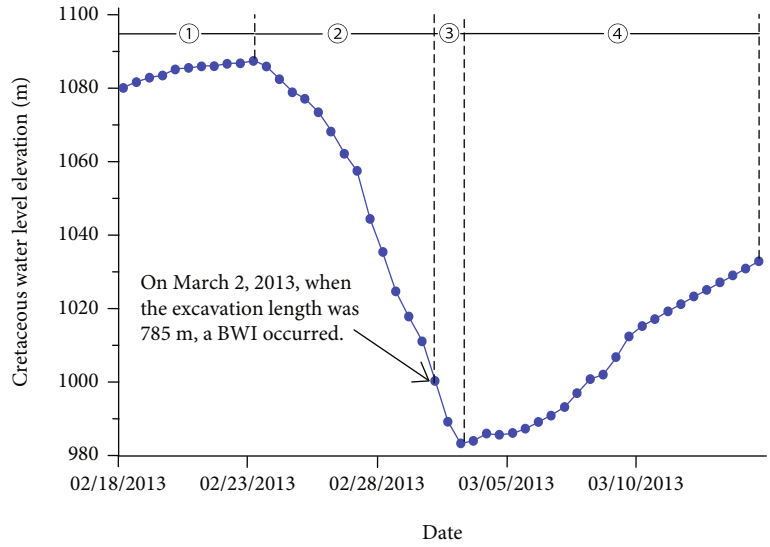

Figure 6: Changes of Cretaceous water level during the formation of a Cretaceous BWI in Cuimu coal mine. ①: natural recovery period of water level; ②: filling period of water in Cretaceous aquifer into bed separation; ③: bed-separation water inrush period; ④: water level recovery period after water inrush channel closure.

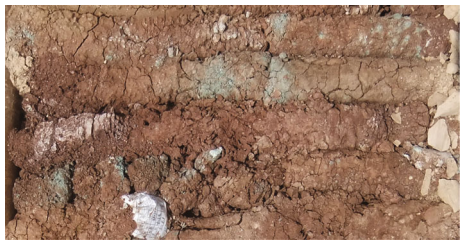

Figure 7: Argillization of Jurassic mudstone core after encountering water.

Figure 8: Disintegration of Jurassic sandstone core after encountering water.

mudstone before mudstone fracture. Therefore, C_m can be quantified by the following formula:

$$C_m = \sum_{i=1}^{n} c_{mi}, \tag{3}$$

$$c_{mi} = \frac{t_{mi}}{\Psi_{mi}} = \frac{t_{mi}}{M - T_{mi} * (\eta - 1)}. \tag{4}$$

where c_{mi}, t_{mi}, and Ψ_{mi} refer to the closure potential, thickness, and height of available settlement space of the i^{th} mudstone layer in FJS, respectively; η refers to the average expansion coefficient of the fractured rock mass, which can be obtained through field monitoring; and T_{mi} refers to the total thickness of all strata between the i^{th} mudstone layer in FJS and the coal seam.

(4) Closure potential of sandstone fractures in FJS (C_s)

Due to the low cementation degree, the Jurassic sandstone is easy to disintegrate after encountering water (Figure 8), and the fractures in the Jurassic sandstone are easy to be filled and closed by the disintegrated rock debris.

In FJS, the better the closure effect of sandstone fractures, the stronger the water-resisting capacity of sandstone, and the smaller the probability of BWI. Here, the closure potential of sandstone fractures in FJS (C_s) was used to evaluate the closure effect of sandstone fractures. Because C_s is positively correlated with the sandstone fracture length and the sandstone fracture length is positively correlated with the sandstone thickness, C_s is positively correlated with the sandstone thickness. On the contrary, because C_s is negatively correlated with the opening degree of sandstone fractures, and the opening degree of sandstone fractures is positively correlated with the height of available subsidence space of sandstone before sandstone fracture, C_s is negatively correlated with the height of available subsidence space of sandstone before sandstone fracture. Therefore, C_s can be quantified by the following formula:

$$C_s = \sum_{i=1}^{n} c_{si}, \tag{5}$$

$$c_{si} = \frac{t_{si}}{\Psi_{si}} = \frac{t_{si}}{M - T_{si} * (\eta - 1)}. \tag{6}$$

where c_{si}, t_{si}, and Ψ_{si} refer to the closure potential, thickness, and height of available settlement space of the i^{th} sandstone layer in FJS, respectively; and T_{si} refers to the total thickness

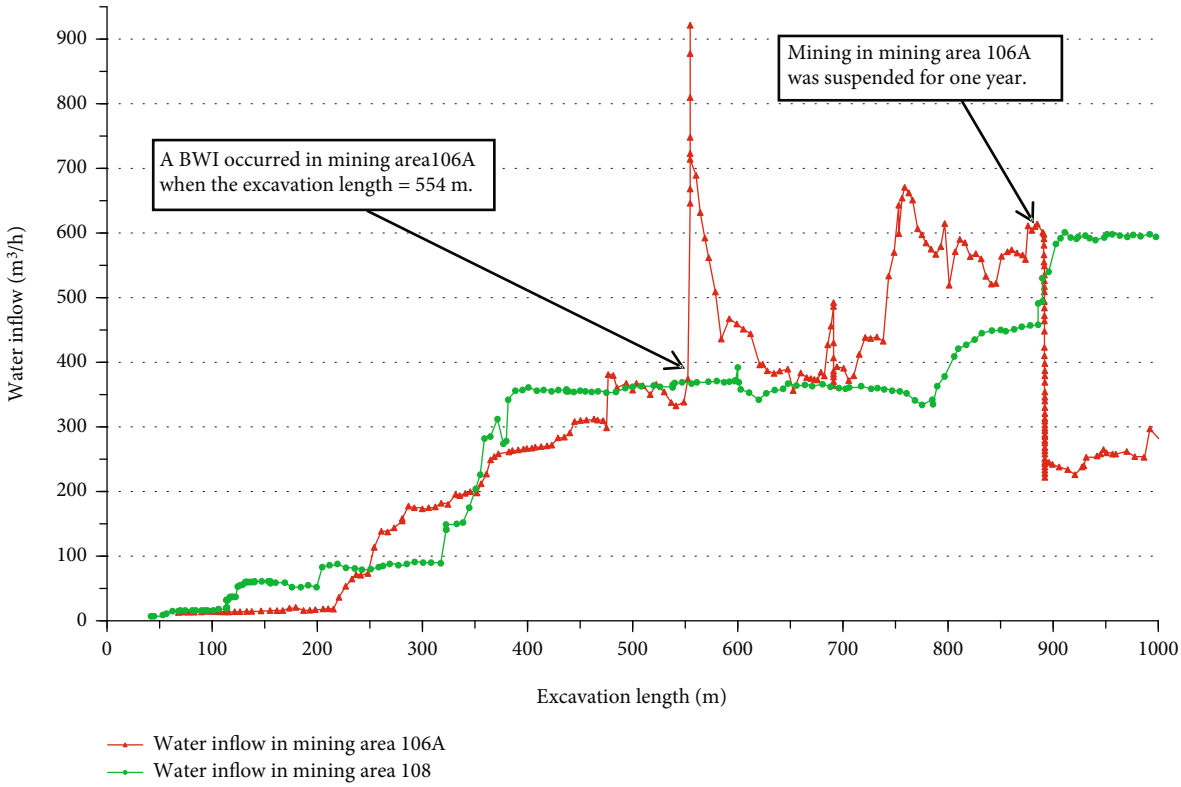

Figure 9: Comparison of water inflow in mining areas 106A and 108 in the Shilawusu coal mine.

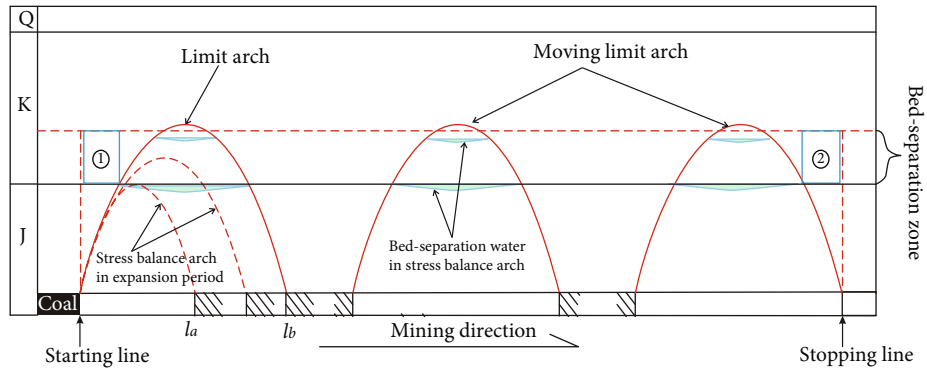

Notes: Q-Quaternary; K-Cretaceous; J-Jurassic;① ② -Out-of-arch zone; *la*-excavation length when stress balance arch just extends to the cretaceous bed-separation zone; *lb*-excavation length when stress balance arch expands to the limit arch.

Figure 10: Schematic diagram of stress balance arches and bed separations in mining disturbed overburden.

of all strata between the i^{th} sandstone layer in FJS and the coal seam.

3.2. Bed-Separation Water Inrush Coefficient (BWIC) Method

3.2.1. Obtaining the BWI-Related Factors at Each Coordinate Point. According to the strata information revealed by each borehole, the values of BWI-related factors in each borehole are calculated. Then, through interpolation calculation, the values of each BWI-related factor at any coordinate point in the area to be evaluated can be obtained. Interpolation calculation can be realized by using a drawing software named Surfer.

3.2.2. Identifying the Weight of Each BWI-Related Factor. UJS with a certain thickness and the same water-resisting capacity as FJS was called the equivalent strata of FJS (E-FJS). In order to calculate the thickness of E-FJS, it is necessary to determine the weight of each BWI-related factor in BWI.

In this paper, the mining areas 106A and 108 in Shilawusu coal mine are taken as examples to explain how to obtain the weight of each BWI-related factor. Mining in

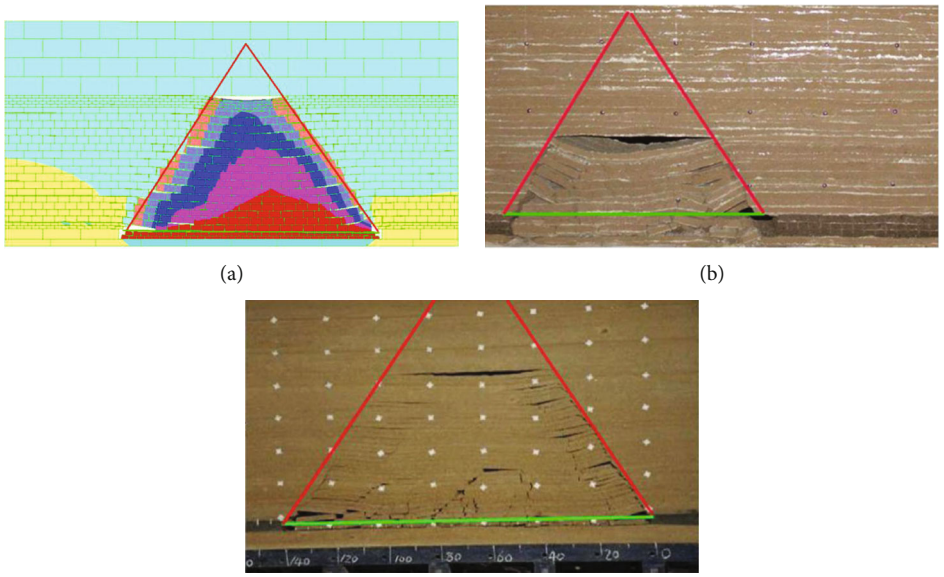

Figure 11: Stress balance arch and its simplification based on some coal seam mining experiments. (a) Numerical simulation experiment of coal seam mining in Cuimu coal mine; (b) similar material simulation experiment of coal seam mining in Buerdong coal mine; (c) similar material simulation experiment of coal seam mining in Daliuta coal mine.

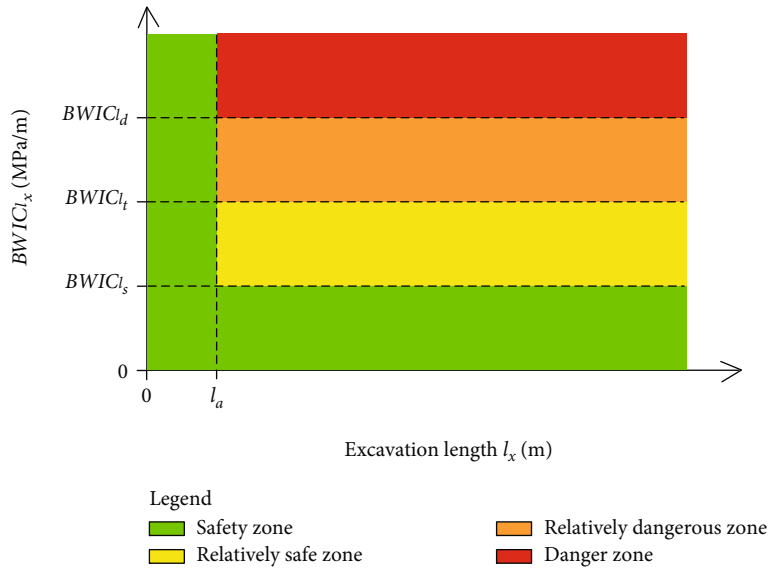

Figure 12: Principle of BWI risk classification based on *BWIC* method.

mining area 106A has been completed, mining in mining area 108 is still in progress, and 1000 m has been excavated. When the excavation length was 554 m, a BWI occurred in mining area 106A, but no BWI occurred in mining area 108 during mining. Because the total amount of water in a bed separation is limited, the water inflow in a BWI has the characteristics of rapid increase and rapid decrease (Figure 9). However, the instantaneous water inflow of BWI is very large, so BWI is very destructive.

Even though mining areas 106A and 108 have the same mining width, similar mining depth, and similar mining thickness, there are differences in BWI-related factors between the two mining areas, which eventually lead to differences in BWI risk between the two mining areas. Therefore, by comparing the differences of BWI-related factors between mining area 106A and mining area 108, the weight of each BWI-related factor in the formation of BWI can be obtained under the premise of excluding the influence of mining width, mining depth, and mining thickness on BWI. The principle of obtaining the weight of each BWI-related factor is consistent with the basic principle of entropy weight method. Therefore, in this paper, entropy weight method was used to obtain the weight of each BWI-related factor.

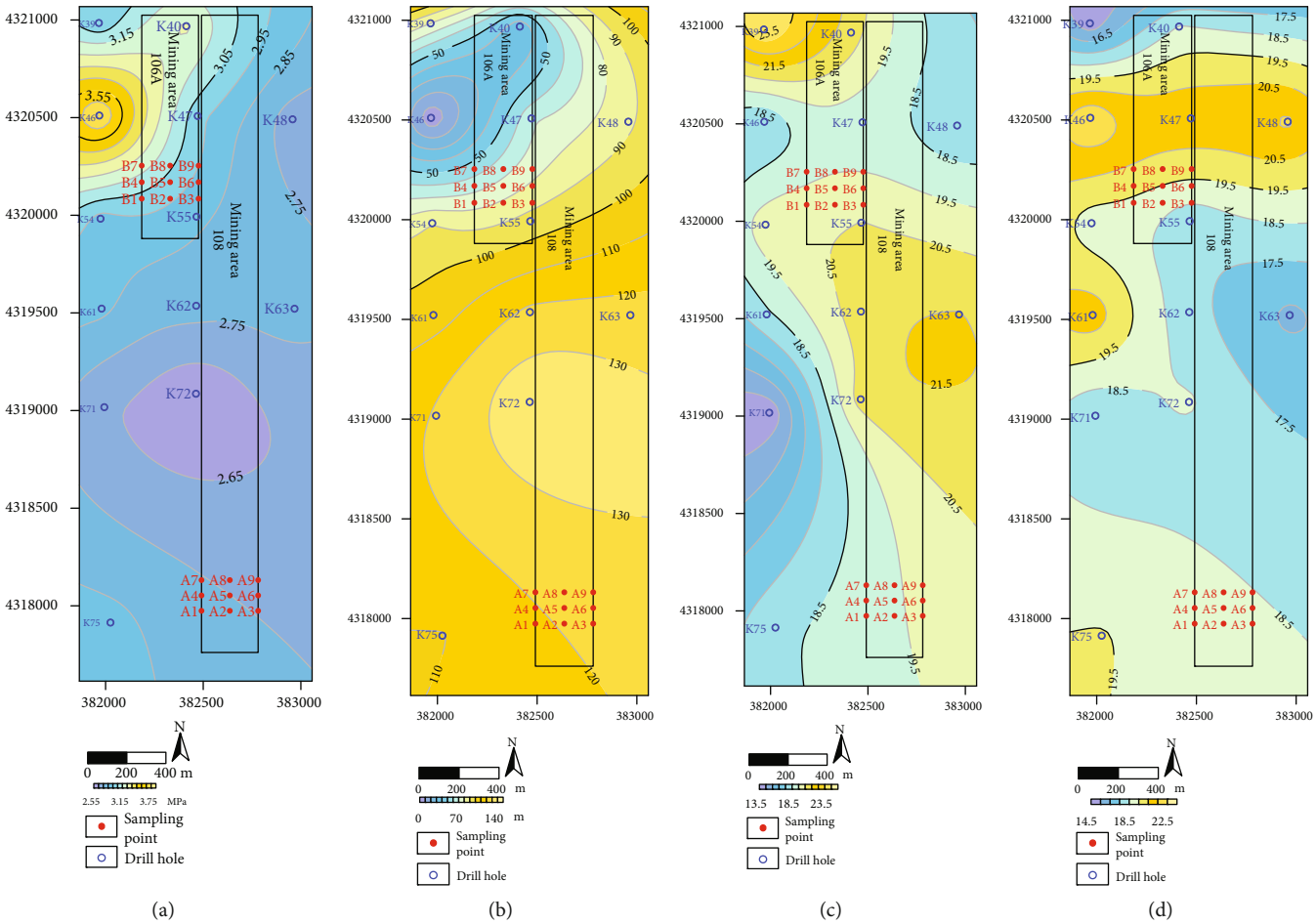

Figure 13: Distribution of (a) P_b, (b) T_U, (c) C_m, and (d) C_s in mining areas 106A and 108 in Shilawusu coal mine.

The data used for weight calculation obtained from m sampling points and n BWI-related factors is written as:

$$X = (x_{ij})_{m\times n} = \begin{pmatrix} x_{11} & \cdots & x_{1n} \\ \vdots & \ddots & \vdots \\ x_{m1} & \cdots & x_{mn} \end{pmatrix}. \tag{7}$$

After standardization, the following results can be obtained:

$$R = (r_{ij})_{m\times n} = \begin{pmatrix} r_{11} & \cdots & r_{1n} \\ \vdots & \ddots & \vdots \\ r_{m1} & \cdots & r_{mn} \end{pmatrix}, \tag{8}$$

where r_{ij} is the standardization value of the i^{th} sampling point for the j^{th} BWI-related factor. For the BWI-related factors positively correlated with BWI, r_{ij} is calculated as follows:

$$r_{ij} = \frac{x_{ij} - \min\limits_{j} x_{ij}}{\max\limits_{j} x_{ij} - \min\limits_{j} x_{ij}}, \tag{9}$$

whereas for the BWI-related factors negatively correlated with BWI, r_{ij} is calculated as follows:

$$r_{ij} = \frac{\max\limits_{j} x_{ij} - x_{ij}}{\max\limits_{j} x_{ij} - \min\limits_{j} x_{ij}}. \tag{10}$$

The information entropy of the j^{th} BWI-related factor (e_j) is defined as:

$$e_j = \frac{-1}{\ln m} \sum_{i=1}^{m} p_{ij} * \ln p_{ij}, \tag{11}$$

where p_{ij} is calculated as follows:

$$p_{ij} = \frac{r_{ij}}{\sum_{i=1}^{m} r_{ij}}. \tag{12}$$

Because when p_{ij} infinitely approaches 0, $p_{ij} * \ln p_{ij}$ approaches 0; here, when $p_{ij} = 0$, the value of $p_{ij} * \ln p_{ij}$ was

Table 1: Values of BWI-related factors at each sampling point.

Sampling points	P_b (MPa)	T_U (m)	C_m	C_s
A1	2.78	119.774	18.858	18.997
A2	2.761	121.818	19.128	18.875
A3	2.746	123.425	19.378	18.767
A4	2.768	120.75	18.829	18.922
A5	2.75	122.759	19.135	18.805
A6	2.737	124.304	19.411	18.699
A7	2.755	121.842	18.799	18.839
A8	2.739	123.791	19.146	18.73
A9	2.726	125.248	19.45	18.628
B1	3.019	77.908	20.419	19.315
B2	2.963	82.763	20.607	18.905
B3	2.898	88.448	20.76	18.539
B4	3.102	68.009	20.08	19.796
B5	3.014	75.583	20.285	19.449
B6	2.925	83.201	20.39	19.213
B7	3.191	57.792	19.726	20.319
B8	3.065	68.571	19.983	20.001
B9	2.95	78.299	20.078	19.832

Table 2: Index weight of BWI-related factors.

BWI-related factors	P_b	T_U	C_m	C_s
Index weight	0.354	0.390	0.158	0.098

Table 3: $T_{E-M-FJS}$ of mudstone at different locations in FJS.

Location	t_m (m)	T_m (m)	c_m	$T_{E-M-FJS}$ (m)	$T_{E-M-FJS}/t_m$
Top of FJS	1	229	0.374	0.763	76.3%
Bottom of FJS	1	0	0.1	0.204	20.4%

Table 4: $T_{E-S-FJS}$ of sandstone at different locations in FJS.

Location	t_s (m)	T_s (m)	c_s	$T_{E-S-FJS}$ (m)	$T_{E-S-FJS}/t_s$
Top of FJS	1	229	0.374	0.487	48.7%
Bottom of FJS	1	0	0.1	0.130	13.0%

set to 0. The entropy weight of the j^{th} BWI-related factor (w_j) can be calculated by the following formula:

$$w_j = \frac{1 - e_j}{n - \sum_{j=1}^{n} e_j}. \tag{13}$$

In this paper, there are four BWI-related factors, so $n = 4$, and w_1, w_2, w_3, and w_4 refer to the weight of P_b, T_U, C_m, and C_s, respectively.

3.2.3. Calculating the E-FJS Thickness (T_{E-FJS}). After calculating the weight of each BWI-related factor in BWI, the

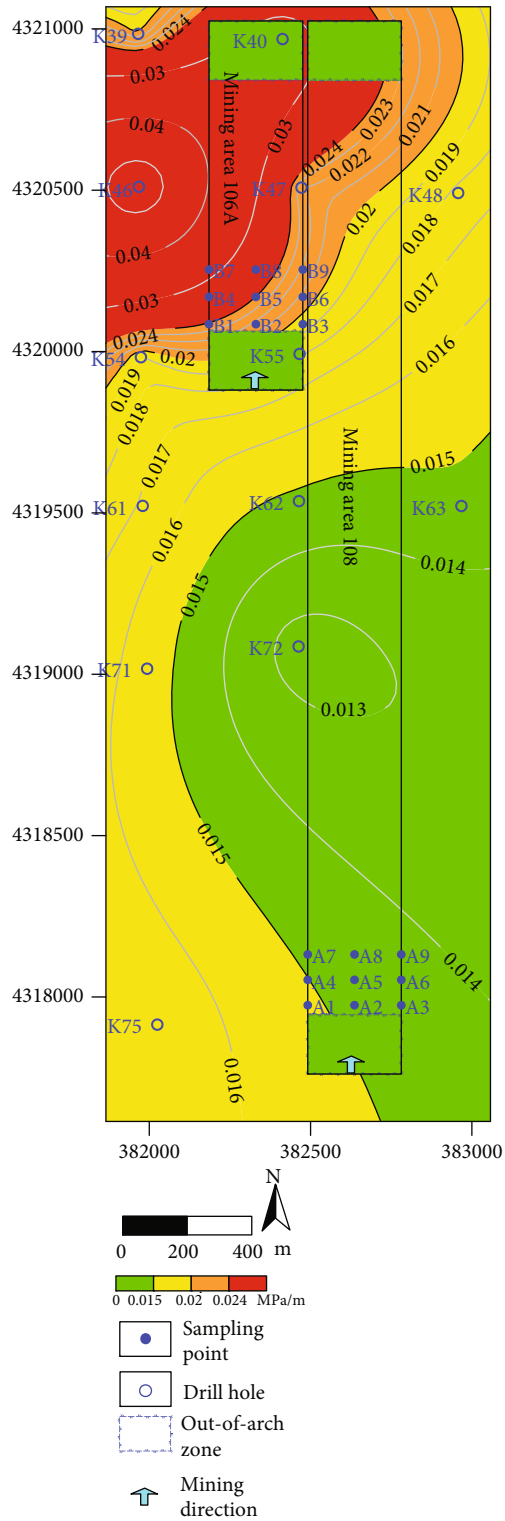

Figure 14: Distribution of *BWIC* in mining areas 106A and 108 in Shilawusu coal mine.

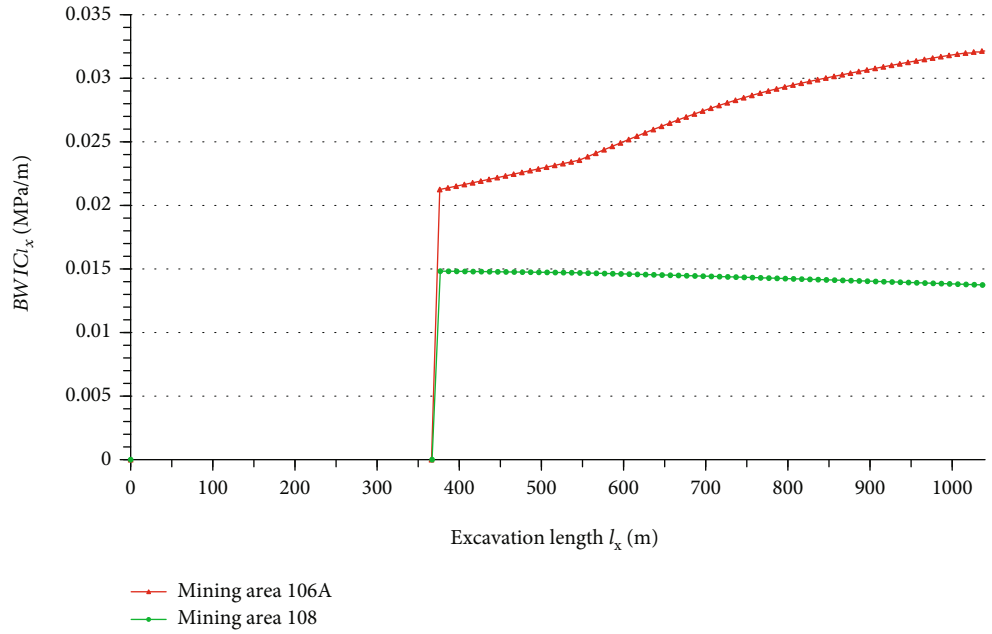

Figure 15: Overall *BWIC* corresponding to different excavation lengths in mining areas 106A and 108 in Shilawusu coal mine.

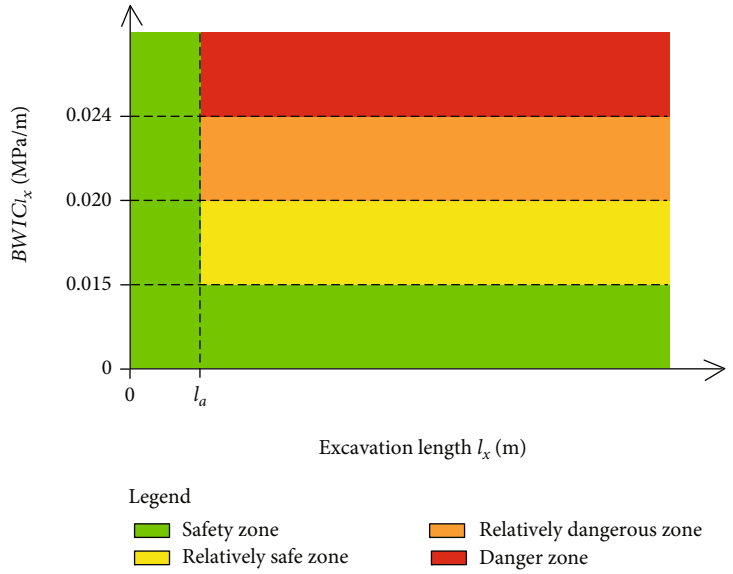

Figure 16: Discriminant diagram of BWI risk classification based on *BWIC* method.

water-resisting capacity index (V_i) of Jurassic protective layer at the i^{th} sampling point can be calculated by the following formula:

$$V_i = \frac{T_{Ui}}{\sum_{i=1}^{m} T_{Ui}} w_2 + \frac{C_{mi}}{\sum_{i=1}^{m} C_{mi}} w_3 + \frac{C_{si}}{\sum_{i=1}^{m} C_{si}} w_4. \quad (14)$$

Equation (14) can be transformed into:

$$V_i = T_{Ui} * k_1 + C_{mi} * k_2 + C_{si} * k_3, \quad (15)$$

where k_1, k_2, and k_3 are constants.

Assuming that the values of T_U, C_m, and C_s at the coordinate point A are T_{UA}, C_{mA}, and C_{sA}, respectively, and the values of T_U, C_m, and C_s at the coordinate point B are T_{UB}, C_{mB}, and C_{sB}, respectively, then according to Equation (15), the water-resisting capacity index of Jurassic protective layer at the coordinate points A and B can be shown as follows:

$$V_A = T_{UA} * k_1 + C_{mA} * k_2 + C_{sA} * k_3, \quad (16)$$

$$V_B = T_{UB} * k_1 + C_{mB} * k_2 + C_{sB} * k_3, \quad (17)$$

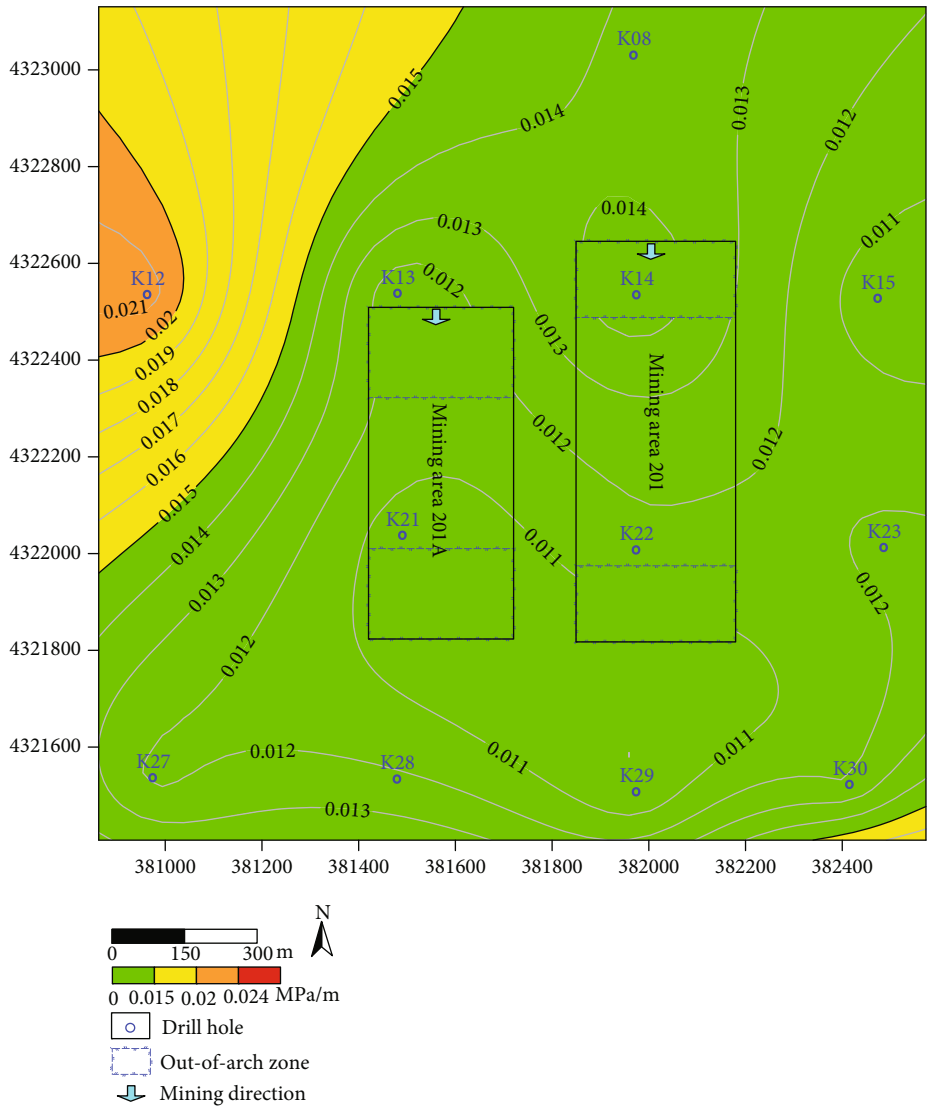

Figure 17: Distribution of *BWIC* in mining areas 201A and 201 in Shilawusu coal mine.

where V_A and V_B are the water-resisting capacity index of Jurassic protective layer at the coordinate points A and B, respectively. Then, the restriction conditions (18) and (19) were set as follows:

$$\begin{cases} V_A = V_B\,; C_{sA} = C_{sB}, \\ T_{UA} \neq 0\,; T_{UB} = 0, \\ C_{mA} = 0\,; C_{mB} \neq 0, \end{cases} \tag{18}$$

$$\begin{cases} V_A = V_B\,; C_{mA} = C_{mB}, \\ T_{UA} \neq 0\,; T_{UB} = 0, \\ C_{sA} = 0\,; C_{sB} \neq 0. \end{cases} \tag{19}$$

By synthesizing Equations (16) and (17) and restriction condition (18), the following equation can be obtained:

$$T_{UA} * k_1 = \left(\frac{k_2}{k_1} * C_{mB}\right) * k_1 = (k_m * C_{mB}) * k_1, \tag{20}$$

where k_m is a constant and its value is the ratio of k_2 to k_1. From Equation (20), it can be concluded that:

$$T_{UA} = k_m * C_{mB}. \tag{21}$$

The physical meaning of Equation (21) can be expressed as when C_m is dimensionless and the unit of T_U is m, the water-resisting capacity of UJS with $T_U = k_m$ m is equal to that of one unit of C_m. UJS with a certain thickness and

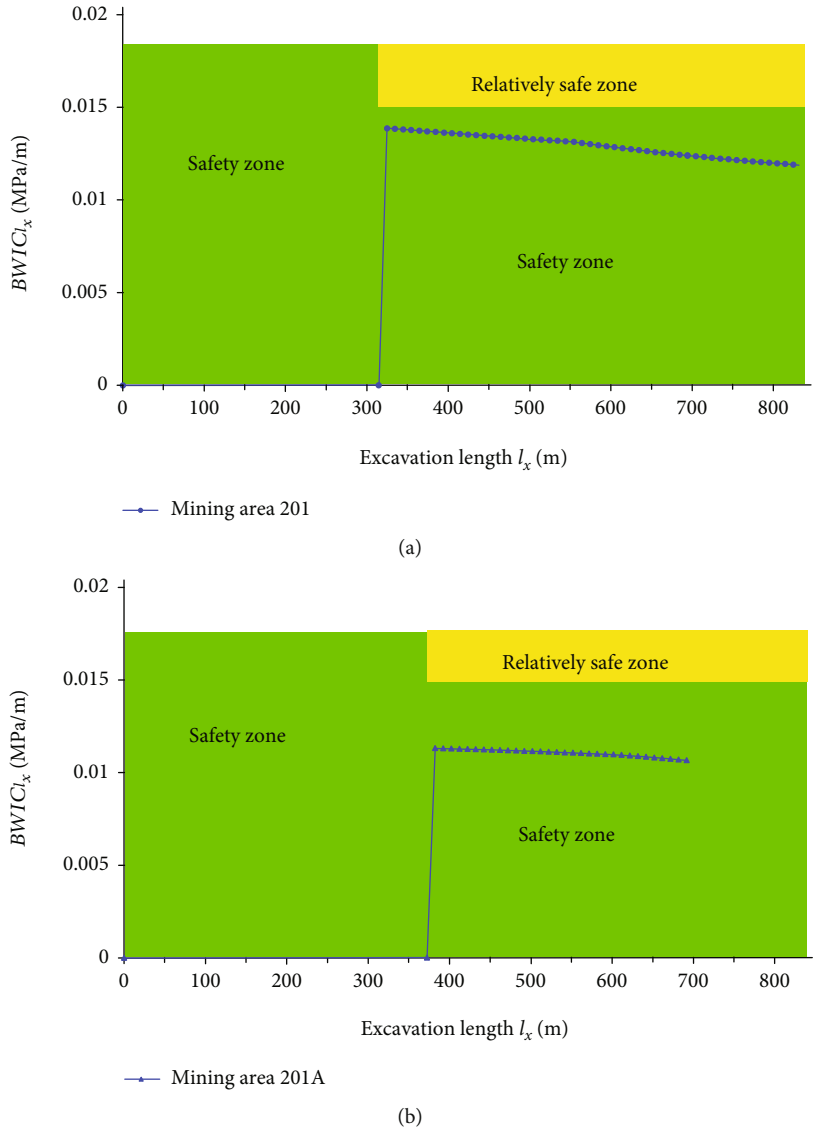

Figure 18: Overall *BWIC* corresponding to different excavation lengths in (a) mining area 201 and (b) mining area 201A in Shilawusu coal mine.

the same water-resisting capacity as mudstone in FJS was called equivalent strata of mudstone in FJS (E-M-FJS). Therefore, the E-M-FJS thickness ($T_{E-M-FJS}$) can be obtained as:

$$T_{E-M-FJS} = k_m * C_m. \tag{22}$$

By synthesizing Equations (16) and (17) and restriction condition (19), the following equation can be obtained:

$$T_{UA} * k_1 = \left(\frac{k_3}{k_1} * C_{sB}\right) * k_1 = (k_s * C_{sB}) * k_1, \tag{23}$$

where k_s is a constant and its value is the ratio of k_3 to k_1. From equation (23), it can be concluded that:

$$T_{UA} = k_s * C_{sB}. \tag{24}$$

The physical meaning of Equation (24) can be expressed as when C_s is dimensionless and the unit of T_U is m, the water-resisting capacity of UJS with $T_U = k_s$ m is equal to that of one unit of C_s. UJS with a certain thickness and the same water-resisting capacity as sandstone in FJS was called equivalent strata of sandstone in FJS (E-S-FJS). Therefore, the E-S-FJS thickness ($T_{E-S-FJS}$) can be obtained as:

$$T_{E-S-FJS} = k_s * C_s. \tag{25}$$

The relationship among T_{E-FJS}, $T_{E-M-FJS}$, and $T_{E-S-FJS}$ satisfies the following equation:

$$T_{E-FJS} = T_{E-M-FJS} + T_{E-S-FJS}. \tag{26}$$

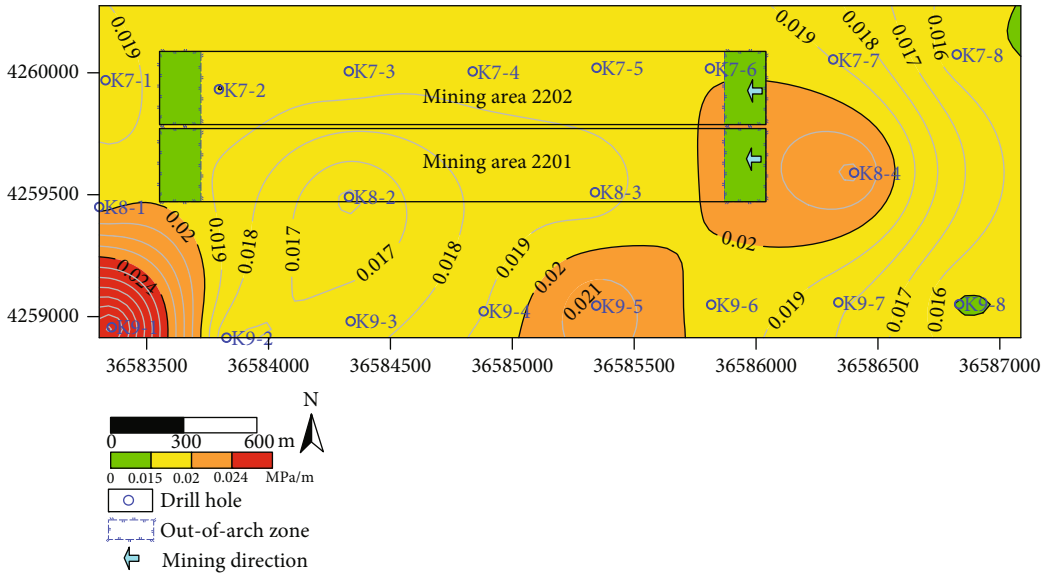

Figure 19: Distribution of *BWIC* in mining areas 2202 and 2201 in Yingpanhao coal mine.

According to Equations (22), (25), and (26), the formula for calculating T_{E-FJS} can be obtained as follows:

$$T_{E-FJS} = k_m * C_m + k_s * C_s. \tag{27}$$

3.2.4. Calculating the BWIC at Each Coordinate Point. The formula for calculating the *BWIC* at each coordinate point (x_i, y_i) can be obtained as follows:

$$BWIC_{(x_i,y_i)} = \frac{P_{b(x_i,y_i)}}{T_{U(x_i,y_i)} + T_{E-FJS(x_i,y_i)}}, \tag{28}$$

where $BWIC_{(x_i,y_i)}$, $P_{b(x_i,y_i)}$, $T_{U(x_i,y_i)}$, and $T_{E-FJS(x_i,y_i)}$, respectively, refer to the *BWIC*, P_b, T_U, and T_{E-FJS} at the coordinate point (x_i, y_i). According to Equation (27), Equation (28) can be transformed into:

$$BWIC_{(x_i,y_i)} = \frac{P_{b(x_i,y_i)}}{T_{U(x_i,y_i)} + k_m * C_{m(x_i,y_i)} + k_s * C_{s(x_i,y_i)}}, \tag{29}$$

where $C_{m(x_i,y_i)}$ and $C_{s(x_i,y_i)}$, respectively, refer to the C_m and C_s at the coordinate point (x_i, y_i).

3.2.5. Obtaining the Overall BWIC Corresponding to Different Excavation Lengths. Since any excavation length corresponds to a stress balance arch (Figure 10), the average *BWIC* in the bed separation zone in the stress balance arch corresponding to each excavation length was used as the overall *BWIC* corresponding to each excavation length. Therefore, the overall BWI risk when the excavation length is l_x can be expressed by the following formula:

$$BWIC_{l_x} = \frac{1}{z} \sum_{i=1}^{z} BWIC_{(x_i,y_i)}, \tag{30}$$

where $BWIC_{l_x}$ and z, respectively, refer to the overall *BWIC* and the number of selected coordinate points within the distribution range of bed separation zone when the excavation length is l_x. In this paper, for the convenience of calculation, z refers to the number of grid points after each bed separation zone distribution range was divided into squares with side length of 10 m.

With the increase of the excavation length, the size of the stress balance arch expands continuously. When the excavation length reaches a specific value, the size of the stress balance arch develops to the maximum, which is called the limit arch. The maximum height of limit arch is about 0.7 times of mining depth. Then, as the excavation continues, the stress balance arch exists in the form of moving arch, which has the same size as the limit arch [17, 18]. In order to observe the shape of the stress balance arch, some mining cases in Cuimu coal mine, Buerdong coal mine, and Daliuta coal mine in Ordos Basin were studied. The mining process of mining area 21301 in Cuimu coal mine was simulated by using the discrete element software UDEC. The results show that the deformed and broken rock strata are located in a triangular area as a whole, the two sides of the triangle are rock fracture lines, and the bottom of the triangle is the distribution range of goaf. In the triangular area, the deformation and fracture degree of the rock stratum below the bed separation is large, while the deformation of the rock stratum above the bed separation is small (Figure 11(a)). Similar material physical simulation experiments of mining cases in Buerdong coal mine and Daliuta coal mine also show that the rock strata that can deform and fracture are located in the triangular area surrounded by the two rock fracture lines and the distribution area of goaf (Figures 11(b) and 11(c)). Because the deformation and failure of overburden occur in the stress balance arch, the area surrounded by the triangle composed of rock fracture lines and goaf can be equivalent to the area in the stress balance arch, that is, the stress

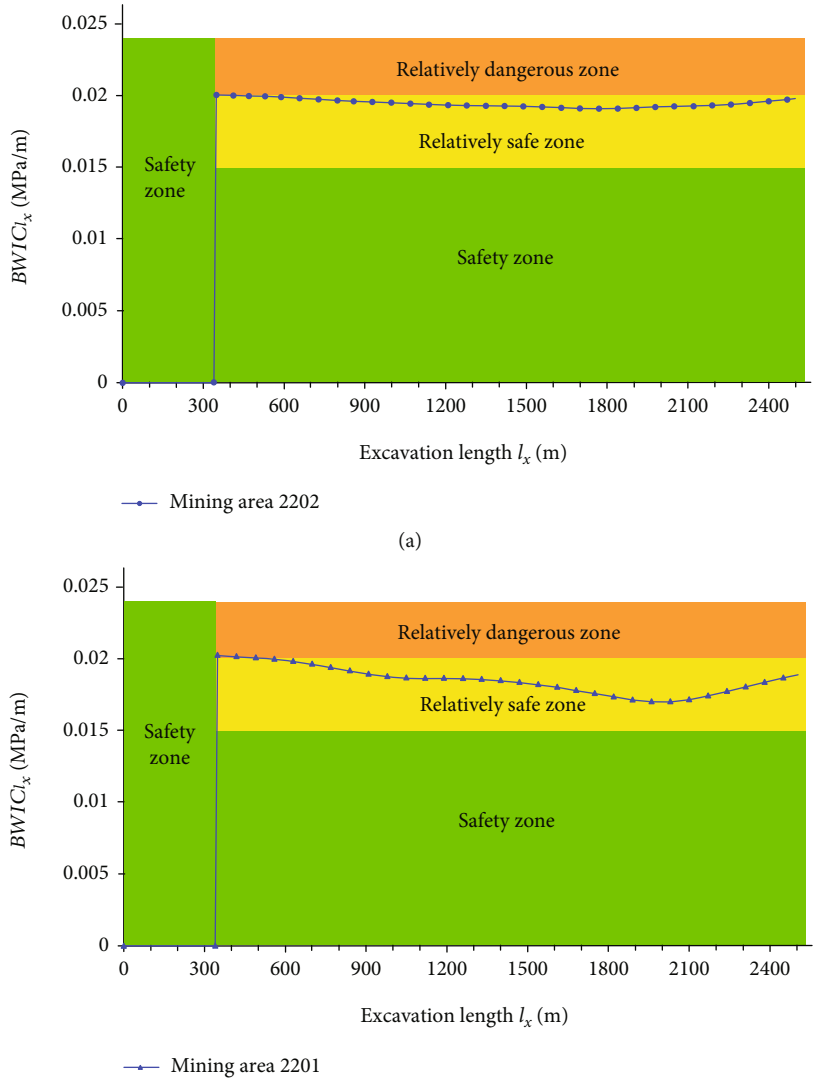

Figure 20: Overall *BWIC* corresponding to different excavation lengths in (a) mining area 2202 and (b) mining area 2201 in Yingpanhao coal mine.

balance arch can be simplified into a triangle with a base angle of about 60° [19, 20].

3.2.6. Grading BWI Risk. In actual mining, the excavation length with or without BWIs is called danger excavation length (l_d) and safety excavation length (l_s), respectively. The $BWIC_{l_x}$ corresponding to l_d and l_s are $BWIC_{l_d}$ and $BWIC_{l_s}$, respectively. $BWIC_{l_x}$ greater than $BWIC_{l_d}$ indicates a high risk of BWI, while $BWIC_{l_x}$ smaller than $BWIC_{l_s}$ indicates a low risk of BWI. Therefore, the risk level with $BWIC_{l_x}$ greater than $BWIC_{l_d}$ was identified as danger, the risk level with $BWIC_{l_x}$ smaller than $BWIC_{l_s}$ was identified as safety, and the risk level with $BWIC_{l_x}$ greater than $BWIC_{l_s}$ less than $BWIC_{l_d}$ was identified as transition. Further division of the transition can be achieved by means of the average value of $BWIC_{l_d}$ and $BWIC_{l_s}$. Here, the average value of $BWIC_{l_d}$ and $BWIC_{l_s}$ was marked as $BWIC_{l_t}$. The risk level with $BWIC_{l_x}$ greater than $BWIC_{l_s}$ less than $BWIC_{l_t}$ was identified as relatively safe, and risk level with $BWIC_{l_x}$ greater than $BWIC_{l_t}$ less than $BWIC_{l_d}$ was identified as relatively dangerous. In addition, when the excavation length is less than l_a, the BWI risk was determined as safe because the stress balance arch has not expanded to the Cretaceous bed separation zone (Figure 10). The principle of BWI risk classification is shown in Figure 12.

4. Results and Discussion

Taking mining areas 106A and 108 in Shilawusu coal mine as examples, the establishment process of *BWIC* method was introduced.

4.1. Obtaining the BWI-Related Factors at Each Coordinate Point. The distribution of related factors in mining areas 106A and 108 in Shilawusu coal mine is shown in Figure 13.

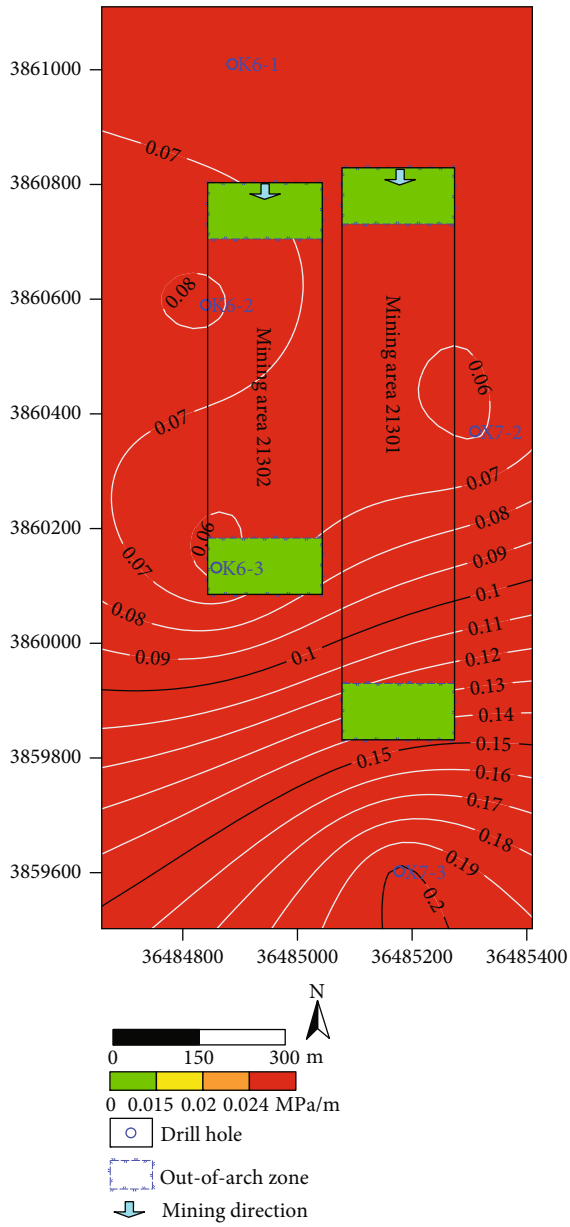

FIGURE 21: Distribution of *BWIC* in mining areas 21301 and 21302 in Cuimu coal mine.

4.2. Identifying the Weight of Each BWI-Related Factor. According to the analysis in Section 3.2, the entropy weight method can be used to determine the weight of BWI-related factors, and the sampling points in mining areas 108 and 106A should be located in the range of the bed separation zone corresponding to the excavation length of 554 m. Based on the triangle stress arch theory, it can be determined that when the excavation length is 554 m, the sampling points in mining area 108 are A1-A9, and the sampling points in mining area 106A are B1-B9 (Figure 13). The values of BWI-related factors at each sampling point are shown in Table 1.

By analyzing the data in Table 1 according to Equations (9)–(13), the weight of each BWI-related factor can be obtained (Table 2).

Because bed-separation water pressure is the power source of BWI, P_b has a large weight. As the integrity of UJS was not damaged, UJS plays an important role in preventing water inrush, so the weight of T_U should be the largest. Because the integrity of the rock strata in FJS has been destroyed, the water-resisting capacity of FJS is still weaker than that of UJS, so the weight of C_m and C_s is less than that of T_U. In addition, because the fracture closure degree of mudstone is relatively better than that of sandstone, the water-resisting capacity of mudstone in FJS is stronger than that of sandstone, so the weight of C_m is greater than that of C_s.

The above analysis results are obtained by reasonable inference based on the actual engineering geological conditions, which are consistent with the results in Table 2, indicating that the calculation results of the weights of BWI-related factors are in line with the reality.

4.3. Calculating the E-FJS Thickness (T_{E-FJS}). According to the weights of BWI-related factors in Table 2, Equation (15) can be expressed as:

$$V_i = 2.186 \times 10^{-4} T_{Ui} + 4.457 \times 10^{-4} C_{mi} + 2.844 \times 10^{-4} C_{si}. \tag{31}$$

It can be seen from Equation (31) that k_1, k_2, and k_3 are 2.186×10^{-4}, 4.457×10^{-4}, and 2.844×10^{-4}, respectively. Then, k_m and k_s can also be calculated, which are 2.039 and 1.301, respectively, and Equations (22) and (25) can be expressed as follows:

$$T_{E-M-FJS} = 2.039 C_m, \tag{32}$$

$$T_{E-S-FJS} = 1.301 C_s, \tag{33}$$

Taking mining area 106A in Shilawusu coal mine as an example, when M, R_{FM}, and η are 10 m, 23, and 1.032, respectively, the $T_{E-M-FJS}$ of mudstone with a thickness of 1 m at different locations in FJS was calculated by using Equations (4) and (32) (Table 3), and the $T_{E-S-FJS}$ of sandstone with a thickness of 1 m at different locations in FJS was calculated by using Equations (6) and (33) (Table 4).

Although the rock in FJS still have water-resisting capacity due to the closure of internal fractures, the restored water-resisting capacity is still weaker than that of the unfractured rock because the integrity of the fractured rock has been destroyed. This conclusion can also be obtained by analyzing the data in Table 3 and Table 4. It can be seen from Table 3 and Table 4 that the water resistance capacity of mudstone and sandstone in FJS is weaker than that of intact rock. Due to the larger opening and weaker closure of the fractures, the water-resisting capacity of the rock at the bottom of FJS is less than that of the rock at the top of FJS. In addition, in FJS, due to the self-healing effect of fractures in mudstone, the fractures in mudstone are easier to close than those in sandstone, so that the water-resisting capacity of mudstone at the same location is stronger than that of sandstone.

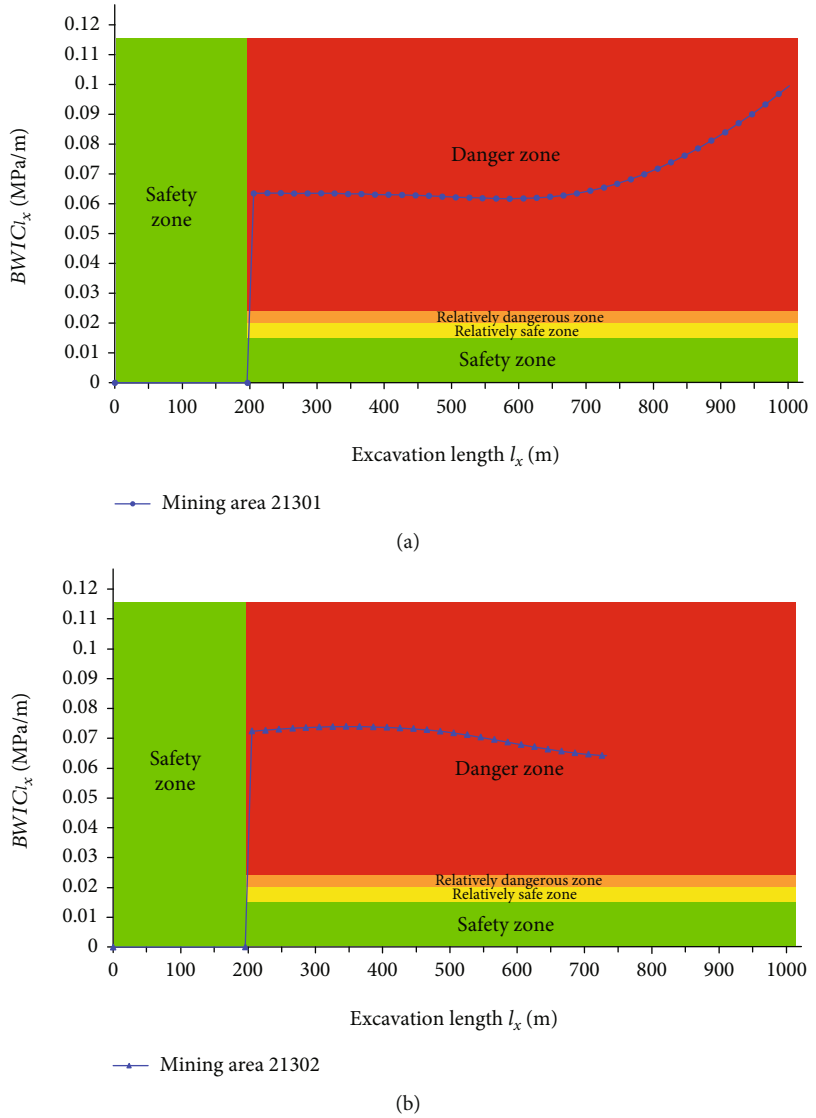

Figure 22: Overall *BWIC* corresponding to different excavation lengths in (a) mining area 21301 and (b) mining area 21302 in Cuimu coal mine.

The above analysis shows that the method of obtaining T_{E-FJS} determined in this paper is practical, and the formula for calculating T_{E-FJS} is as follows:

$$T_{E-FJS} = 2.039C_m + 1.301C_s. \quad (34)$$

4.4. Calculating the BWIC at Each Coordinate Point. Since k_m and k_s are 2.039 and 1.301, respectively, Equation (29) can be transformed into:

$$BWIC_{(x_i,y_i)} = \frac{P_{b(x_i,y_i)}}{T_{U(x_i,y_i)} + 2.039C_{m(x_i,y_i)} + 1.301C_{s(x_i,y_i)}}, \quad (35)$$

According to formula (35), the *BWIC* at each coordinate point in mining areas 108 and 106A can be obtained (Figure 14).

4.5. Obtaining the Overall BWIC Corresponding to Different Excavation Lengths. Based on the triangle stress arch theory, the overall *BWIC* corresponding to different excavation lengths can be obtained by using Equations (30) and (35) (Figure 15).

4.6. Grading BWI Risk. Because BWI occurred in mining area 106A when $l_x = 554$ m, but no BWI occurred in the completed 1000 m mining process in mining area 108, the $BWIC_{l_x}$ corresponding to the excavation length of 554 m in mining area 106A was regarded as $BWIC_{l_d}$, and the maximum value of $BWIC_{l_x}$ in mining area 108 was used as $BWIC_{l_s}$. According to Figure 15, $BWIC_{l_d} = 0.024$ MPa/m, $BWIC_{l_s} = 0.015$ MPa/m, so $BWIC_{l_t} = 0.020$ MPa/m. Therefore, Figure 12 can be improved to Figure 16.

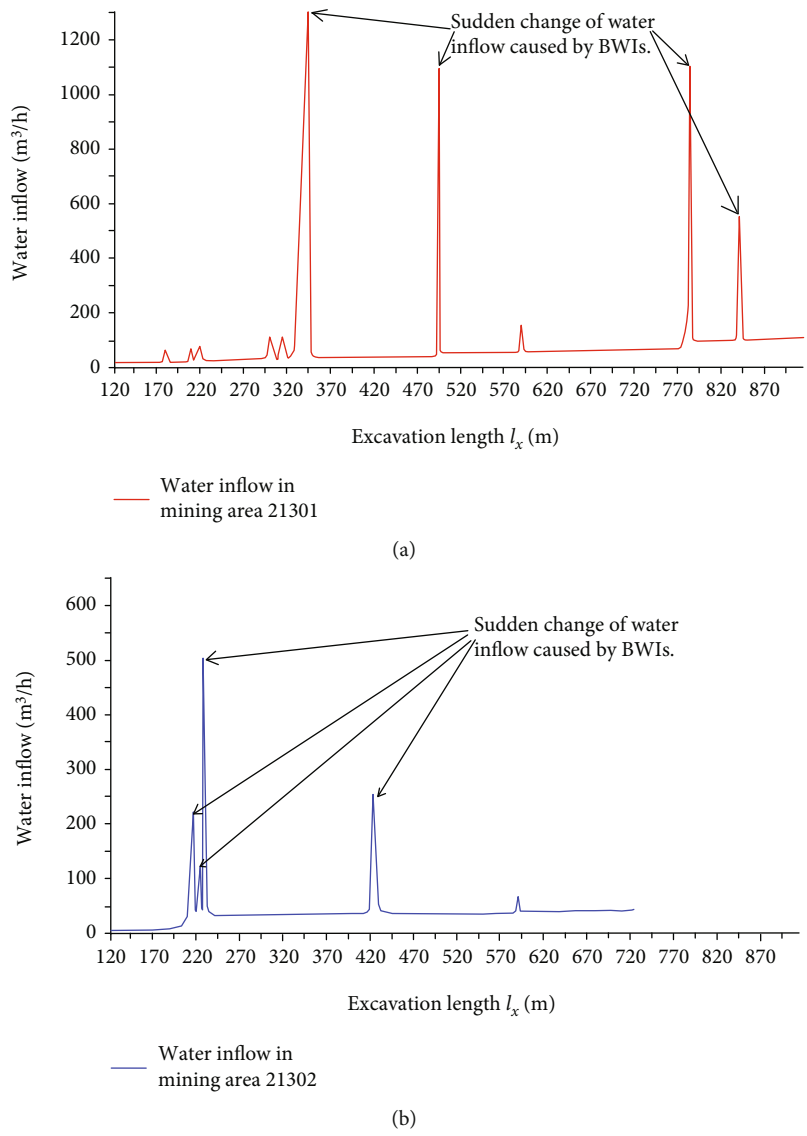

Figure 23: Water inflow in (a) mining area 21301 and (b) mining area 21302 in Cuimu coal mine.

5. Application and Validation

5.1. Shilawusu Coal Mine. According to formula (35), the *BWIC* at each coordinate point in mining areas 201 and 201A in Shilawusu coal mine can be obtained (Figure 17). Based on the triangle stress arch theory, the overall *BWIC* corresponding to different excavation lengths can be obtained by using Equations (30) and (35) (Figure 18). It can be seen from Figure 18 that the BWI risk in mining areas 201 and 201A during mining belongs to the "safety zone." In fact, the mining in mining areas 201 and 201A has been completed, and no BWI occurred during mining, which verifies the accuracy of the evaluation results shown in Figure 18.

5.2. Yingpanhao Coal Mine. According to formula (35), the *BWIC* at each coordinate point in mining areas 2202 and 2201 in Yingpanhao coal mine can be obtained (Figure 19). Based on the triangle stress arch theory, the overall *BWIC* corresponding to different excavation lengths can be obtained by using Equations (30) and (35) (Figure 20). It can be seen from Figure 20 that the BWI risk in mining areas 2202 and 2201 during mining belongs to the "relatively safe zone." In fact, mining has been completed in mining area 2201, and 1000 m excavation has been completed in mining area 2202. No BWI occurred during mining in these two mining areas, which verifies the accuracy of the assessment results shown in Figure 20.

5.3. Cuimu Coal Mine. According to formula (35), the *BWIC* at each coordinate point in mining areas 21301 and 21302 in Cuimu coal mine can be obtained (Figure 21). Based on the triangle stress arch theory, the overall *BWIC* corresponding to different excavation lengths can be obtained by using Equations (30) and (35) (Figure 22). It can be seen from Figure 22 that the BWI risk in mining areas 21301 and 21302 during mining belongs to the "danger zone." In fact, the mining in mining areas 21301 and 21302 has been

completed, and BWIs occurred during mining (Figure 23), which verifies the accuracy of the evaluation results shown in Figure 22.

6. Conclusions

The objects directly involved in BWI process include the Cretaceous bed-separation water and the Jurassic protective layer. The bed-separation water pressure (P_b) provides the inducing power for the occurrence of BWI and can be expressed by the water pressure in the aquifer at the bottom of Cretaceous. In the Jurassic protective layer, the upper part is the unbroken Jurassic strata (UJS), and the lower part is the fractured Jurassic strata (FJS). The water-resisting capacity of FJS is due to the closure of fractures in FJS under the action of water flow.

The greater the UJS thickness (T_U) is, the stronger its water-resisting capacity is. In FJS, the closure potential of mudstone fractures (C_m) was used to evaluate the closure effect of mudstone fractures, and the closure potential of sandstone fractures (C_s) was used to evaluate the closure effect of sandstone fractures. C_m is positively correlated with the mudstone thickness and negatively correlated with the height of available subsidence space of mudstone before mudstone fracture. C_s is positively correlated with the sandstone thickness, and negatively correlated with the height of available subsidence space of sandstone before sandstone fracture. UJS with a certain thickness and the same water-resisting capacity as mudstone in FJS was called equivalent strata of mudstone in FJS (E-M-FJS). UJS with a certain thickness and the same water-resisting capacity as sandstone in FJS was called equivalent strata of sandstone in FJS (E-S-FJS). By comparing the weight of each BWI-related factor, the formulas for calculating the E-M-FJS thickness ($T_{E-M-FJS}$) and the E-S-FJS thickness ($T_{E-S-FJS}$) were derived. And the $T_{E-M-FJS}$ corresponding to one unit of C_m is 2.039 m, while the $T_{E-S-FJS}$ corresponding to one unit of C_s is 1.301 m. The weight of each BWI-related factor was obtained by entropy weight method. And the weights of P_b, T_U, C_m, and C_s are 0.354, 0.390, 0.158, and 0.098, respectively.

In bed-separation water inrush (BWI) risk assessment, the existing multifactor-weighted superposition method cannot provide a universal risk classification standard, and the existing water inrush coefficient method ignores the water separation capacity of FJS, so there is still a lack of scientific BWI risk assessment method. In this paper, three coal mines in Ordos Basin were taken as research cases, and a bed-separation water inrush coefficient (*BWIC*) method for BWI risk assessment was established. The value of *BWIC* is the ratio of P_b to the sum of T_U, $T_{E-M-FJS}$ and $T_{E-S-FJS}$. Based on the stress arch theory, the overall *BWIC* in bed separation zone corresponding to different excavation lengths ($BWIC_{l_x}$) was obtained. By comparing the value range of BWIC_{l_x} with and without BWI, the standard of BWI risk classification was determined. In the BWI risk classification discrimination diagram established based on *BWIC* method, the area with $0\,\mathrm{MPa/m} < BWIC_{l_x} \le 0.015\,\mathrm{MPa/m}$ was divided into safety zone, the area with $0.015\,\mathrm{MPa/m} < BWIC_{l_x} \le 0.02\,\mathrm{MPa/m}$ was divided into relatively safe zone, the area with $0.02\,\mathrm{MPa/m} < BWIC_{l_x} \le 0.024\,\mathrm{MPa/m}$ was divided into relatively dangerous zone, and the area with $BWIC_{l_x} > 0.024\,\mathrm{MPa/m}$ was divided into danger zone. The application results verified the scientificity of *BWIC* method and the universality of the BWI risk classification standard proposed in this paper.

Data Availability

The authors confirm that the data supporting the findings of this study are available within the article.

Conflicts of Interest

The authors declare that they have no conflicts of interest.

Acknowledgments

The authors are grateful to the many people who assisted with this study. The study was jointly supported by the Scientific Research Start-Up Fund for High-Level Introduced Talents of Anhui University of Science and Technology (grant no. 2022yjrc21), the Key Projects of the Natural Science Foundation of China (grant no. 41931284), the China Postdoctoral Science Foundation (grant no. 2019M652015), and the Natural Science Foundation of Jiangsu Province (grant no. BK20190646).

References

[1] J. H. He, W. P. Li, Y. Liu, Z. Yang, S. L. Liu, and L. F. Li, "An improved method for determining the position of overlying separated strata in mining," *Engineering Failure Analysis*, vol. 83, pp. 17–29, 2018.

[2] V. Palchik, "Formation of fractured zones in overburden due to longwall mining," *Environmental Geology*, vol. 44, no. 1, pp. 28–38, 2003.

[3] V. Palchik, "Localization of mining-induced horizontal fractures along rock layer interfaces in overburden: field measurements and prediction," *Environmental Geology*, vol. 48, no. 1, pp. 68–80, 2005.

[4] S. S. Peng, *Longwall mining*, Science Press, Morgantown, 2006.

[5] X. L. Xu, N. Zhang, and S. C. Tian, "Mining-induced movement properties and fissure time-space evolution law in overlying strata," *International Journal of Mining Science and Technology*, vol. 22, no. 6, pp. 817–820, 2012.

[6] H. R. Gui and M. L. Lin, "Types of water hazards in China coalmines and regional characteristics," *Natural Hazards*, vol. 84, no. 2, pp. 1501–1512, 2016.

[7] S. L. Liu and W. P. Li, "Indicators sensitivity analysis for environmental engineering geological patterns caused by underground coal mining with integrating variable weight theory and improved matter-element extension model," *Science of the Total Environment*, vol. 686, pp. 606–618, 2019.

[8] S. L. Liu, W. P. Li, and Q. Q. Wang, "Zoning method for environmental engineering geological patterns in underground coal mining areas," *Science of the Total Environment*, vol. 634, pp. 1064–1076, 2018.

[9] H. J. Li, Q. T. Chen, Z. Y. Shu, L. Li, and Y. C. Zhang, "On prevention and mechanism of bed-separation water inrush for thick coal seams: a case study in China," *Environmental Earth Sciences*, vol. 77, no. 22, article 759, 2018.

[10] X. Q. Li, *Study on the inrush mechanism of the water in bed separation due to repeated coal mining under hard rock*, China University of Mining and Technology, Xuzhou, 2011.

[11] R. Hu, J. W. Wu, X. R. Zhai, and W. Liu, "Recognition and prevention of bed-separation water: based on trapezoid platform model," *Geofluids*, vol. 2021, Article ID 6626268, 10 pages, 2021.

[12] J. G. Xu, D. L. Zhao, and J. H. He, "Mechanism of water inrush in overlying strata of cretaceous thick sandstone," *Safety in Coal Mines*, vol. 51, no. 2, pp. 58–63, 2020.

[13] S. N. Dong, Y. D. Ji, H. Wang et al., "Prevention and control technology and application of roof water disaster in Jurassic coal field of Ordos Basin," *Journal of China Coal Society*, vol. 45, no. 7, pp. 2367–2375, 2020.

[14] Q. Y. Lu, X. Q. Li, W. P. Li, W. Chen, L. F. Li, and S. L. Liu, "Risk evaluation of bed-separation water inrush: a case study in the Yangliu coal mine China," *Mine Water and the Environment*, vol. 37, no. 2, pp. 288–299, 2018.

[15] Q. Y. Lu, *Risk Prediction and Evaluation of Bed-Separation Water Inrush Caused by Breakage of Hard Overburden: a Case Studied in Yangliu Coal Mine*, China University of Mining and Technology, Xuzhou, 2019.

[16] K. F. Fan, W. P. Li, Q. Q. Wang et al., "Formation mechanism and prediction method of water inrush from separated layers within coal seam mining: a case study in the Shilawusu mining area, China," *Engineering Failure Analysis*, vol. 103, pp. 158–172, 2019.

[17] Z. J. Su, *Research of Deformation Mechanism of Mining Overburden Separated Strata*, Liaoning Technical University, Fuxin, 2001.

[18] Z. J. Su, G. M. Yu, and L. Yang, "Numerical simulation on mechanism of deformation of separated strata in overburden," *Chinese Journal of Rock Mechanics and Engineering*, vol. 22, no. 8, pp. 1287–1290, 2003.

[19] J. H. He, *Dynamic Evolution of Bed Separation in Coal Seam Mining and Assessment of Bed-Separation Water Hazards*, PhD He, China University of Mining and Technology, Chinese, 2018.

[20] J. H. He, W. P. Li, and W. Qiao, "A rock mechanics calculation model for identifying bed separation position and analyzing overburden breakage in mining," *Arabian Journal of Geosciences*, vol. 13, no. 18, article 920, 2020.